

NEW 28-GHz SUPERCONDUCTING ELECTRON CYCLOTRON RESONANCE ION SOURCE FOR SYNTHESIZING SUPER-HEAVY ELEMENTS WITH $Z > 118$

T. Nagatomo[†], Y. Higurashi, J. Ohnishi, A. Uchiyama, K. Kumagai, M. Fujimaki, N. Fukunishi, N. Sakamoto, T. Nakagawa and O. Kamigaito

RIKEN Nishina Center for Accelerator Based Science, Wako, Saitama 351-0198, Japan

Abstract

The RIKEN linear accelerator is being upgraded to provide intense metal ion beams, from Ca and Zn for nuclear structure research to V and Cr for synthesizing new super-heavy elements with $Z > 118$. In 2017, we started to construct a new superconducting electron cyclotron resonance ion source (SC-ECRIS) and a new low-energy beam transport (LEBT). Because of the short development period, we decided to give the new SC-ECRIS the same structure as the RIKEN 28-GHz SC-ECRIS. Although a solenoid and some steering magnets were not ready yet, during summer 2018, an ^{40}Ar beam was successfully extracted as the first beam with the 18-GHz microwave heat source. A pepper-pot emittance meter estimated the horizontal size of the $\text{Ar}^{8+, 9+, 11+}$ beam to be about 70 mm at 1,024 mm downstream from the edge of the analyzing magnet. Furthermore, we successfully obtained the four-dimensional phase-space distribution that is essential for evaluating the validity of the beam optics devices to improve the LEBT. We plan to finish the construction of a 28-GHz gyrotron and the LEBT by the end of 2018.

INTRODUCTION

A project to synthesize new super-heavy elements (SHEs) having an atomic number (Z) larger than 118 was

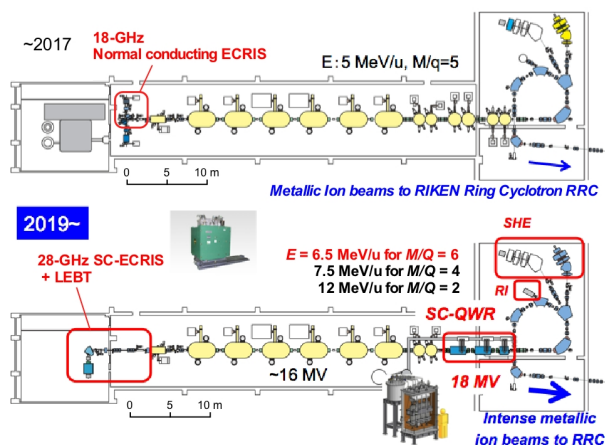


Figure 1: Ongoing upgrade of RILAC since 2017. The normal conducting 18-GHz ECRIS is being replaced with a 28-GHz ECRIS and LEBT. The new SC-QWRs will be installed at the end of drift tubes of the RILAC.

[†] nagatomo@riken.jp

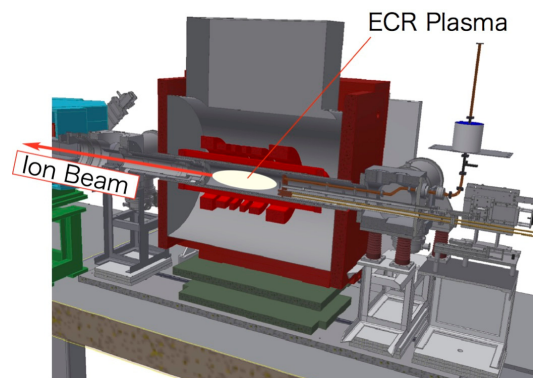


Figure 2: Schematic of the new 28-GHz SC-ECRIS.

started in FY2016. To synthesize SHEs with atomic numbers of $Z = 119$ and 120 , highly intense and highly charged metallic ion beams of V and Cr, respectively, must be provided by the RIKEN linear accelerator (RILAC) [1]. Accordingly, the RILAC upgrade will increase the acceleration energy from 5 MeV/u to more than 6 MeV/u by installing superconducting quarter-wavelength resonators (SC-QWRs), as shown in Fig. 1. However, the RILAC is currently used as a variable-frequency injector for the RIKEN cascaded cyclotron for the Radioactive Isotope Beam Factory [2]. In this operation, the new SC-QWRs will be bypassed because they operate at a fixed frequency. In variable frequency operation, high-intensity Ca and Zn beams will still be required for nuclear structure research, as before. To meet this acceleration scheme without using the SC-QWR booster, the accelerated ions must be given an electric charge higher than that used before. For example, a Ca^{16+} beam is required at currents of $\sim 100 \mu\text{A}$.

Consequently, a wide $n_e\tau_i$ range of $\sim 5 \times 10^8$ to $\sim 5 \times 10^9 \text{ cm}^{-3} \text{ s}$ must be covered, where n_e is the electron density and τ_i is the ion confinement time in the plasma [3] in the ion source. In addition, the development period is limited to about one year. Therefore, we decided to construct the new ion source with the same structure as the RIKEN 28-GHz SC-ECRIS [4,5] and match the new low-energy beam transport (LEBT) to the RILAC radio frequency quadrupole (RFQ).

In this paper, we report the current construction status and describe the first beam extraction, which was performed during the summer of 2018.

Content from this work may be used under the terms of the CC BY 3.0 licence (© 2018). Any distribution of this work must maintain attribution to the author(s), title of the work, publisher, and DOI.

THE NEW SC-ECRIS

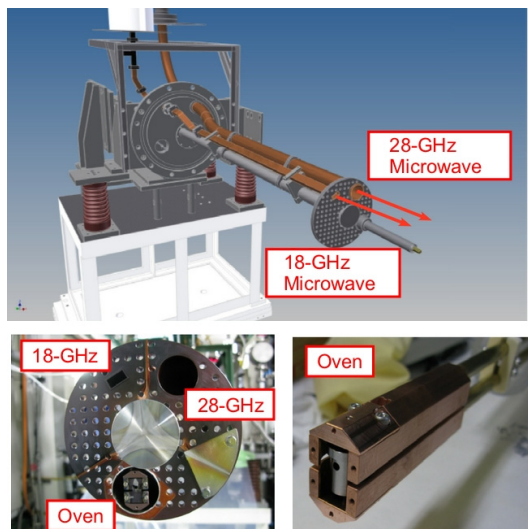


Figure 3: Microwave injection system and high-temperature oven to create metallic ion vapor.

The new ECRIS comprises fully superconducting mirror coils that have the same structure as the RIKEN 28-GHz SC-ECRIS [4]. As shown in Fig. 2, it consists of six solenoidal and hexapole SC magnets that are designed to achieve maximum mirror fields of $B_{inj} \approx 3.8$ T at the microwave injection side and $B_{ext} \approx 2.2$ T at the beam extraction side, a minimum field of $B_{min} < 1.0$ T, and a radial magnetic field at the inside surface of the plasma chamber of $B_r \approx 2.1$ T. The electron plasma confined in the mirror field is heated with 18-GHz and 28-GHz microwaves by the ECR process. Another feature of the ECRIS is that we can use the six solenoidal coils to flexibly change the shape of the ECR surface to create both the “classical” and the “flat” B_{min} structures proposed by Alton et al. [6]. The chamber volume is about 10 L. Schematics of the microwave- and gas-injection systems are shown in Fig. 3. We plan to utilize 18-GHz and 28-GHz microwave heating to generate a high-temperature electron plasma, and these microwaves are generated by a 1.5-kW klystron and a 5-kW gyrotron, respectively. A compact high-temperature (HT) oven, which has a crucible made of thin tungsten and is heated by Joule heating,

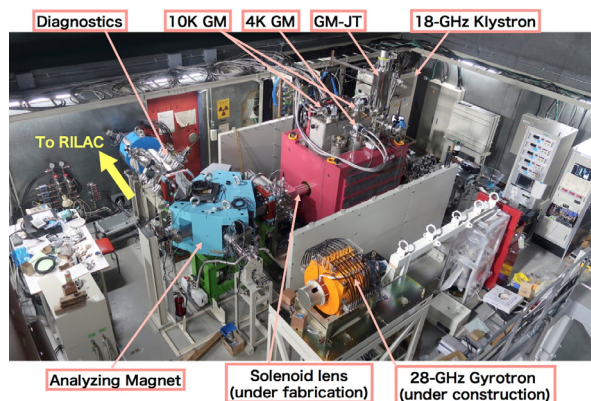


Figure 4: Current construction status of the new 28-GHz ECRIS. The 28-GHz gyrotron and the solenoid lens at the exit of ECRIS is under construction.

was recently developed by Ohnishi et al. [7], and a high-intensity V beam was successfully extracted [3]. We plan to install similar compact HT ovens to create ion vapors of metals such as Ca, Ti, Cr, and Zn in the future.

EXPERIMENTAL SETUP FOR FIRST ARGON BEAM EXTRACTION

The current construction status of the new 28-GHz ECRIS is shown in Fig. 4. Two 10-K GM, one 4-K GM, and one GM-JT cryocoolers were installed in the ECRIS as shown in Fig. 4. The 18-GHz klystron, an analyzing magnet (AM), and a diagnostics chamber were also installed. The pole pieces of the analyzing magnet were specifically shaped to cancel the higher-order magnetic component proposed by Leitner et al. [8]. In the diagnostics chamber, a pepper-pot emittance meter (PEEM) that we previously developed [9] is located 1,024 mm downstream from the edge of the AM. By using the PEEM, four-dimensional phase-space information $\{x, y, x', y', \text{intensity}\}$ can be obtained simultaneously. The Faraday cup is located 420 mm behind the PEEM, and between the PEEM and the Faraday cup a horizontal slit with a 40-mm opening is installed. Two steering magnets were already installed, but their power supplies were not ready for the first extraction. The 28-GHz gyrotron and a solenoid lens that will be placed at the end of the ECRIS are now under construction, and their installation is planned by the end of 2018. Thus, we performed beam extraction with 18-GHz microwave heating with the ^{40}Ar and $^{16}\text{O}_2$ support gas injected into the plasma chamber.

The ^{40}Ar beam was successfully extracted from the new 28-GHz ECRIS on August 9, 2018, as the first beam, and the M/Q spectrum was obtained as shown in Fig. 5. By tuning the ECRIS parameters, we optimized the $^{40}\text{Ar}^{11+}$ beam current with an 18-GHz microwave power of 600 W and an extraction voltage of 15 kV. The maximum $^{40}\text{Ar}^{11+}$ beam current was about 90 μA , and the drain current in the plasma chamber was about 1.8 mA. The beam current was not as high as expected, and we attributed this to the non-optimized beam transport because of the missing magnets described above.

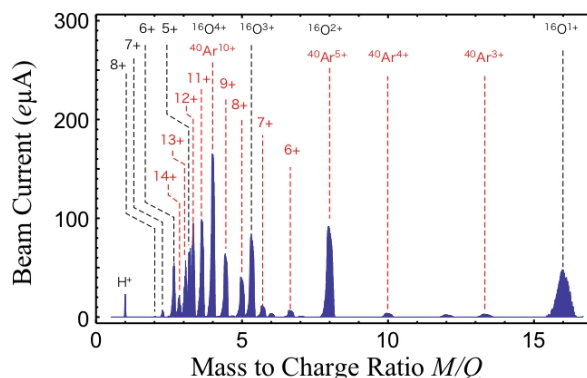


Figure 5: The M/Q spectrum of a ^{40}Ar beam with $^{16}\text{O}_2$ support gas utilizing 18-GHz microwaves with a power of 600 W.

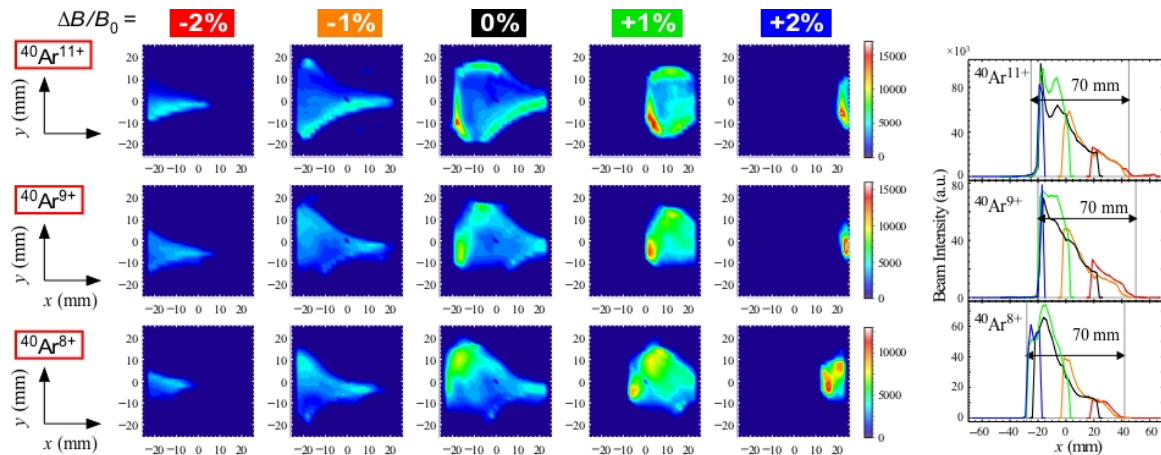


Figure 6: The contour plots on the left show $^{40}\text{Ar}^{11+, 9+, 8+}$ beam profiles obtained using the PPEM with analyzing magnetic field deviations of -2% to $+2\%$. On the right, the beam intensity is projected along the horizontal axis. The color of the projection line indicates the deviation of the magnetic field relative to that for the central trajectory B_0 ; the blue, green, black, orange, and red curves correspond to $\Delta B/B_0 = +2\%$, $+1\%$, 0% , -1% , and -2% , respectively.

We used the PPEM to obtain the $^{40}\text{Ar}^{8+, 9+, 11+}$ beam profiles shown in Fig. 6. From the center column of Fig. 6, the beam size seems to exceed the PPEM scope of an area $5\text{ cm} \times 5\text{ cm}$ square. Thus, we changed the magnetic field of the AM from -2% to $+2\%$ with respect to that of the center trajectory B_0 . By accounting for the position shift corresponding to the magnetic field deviation at the position of the PPEM, the projections of the intensity on the horizontal axis x for each charge state are shown in the right column in Fig. 6. For each charge state, the obtained curves are connected smoothly without any correction, except for the black curves obtained with $B/B_0 = 0\%$. This is reasonable because the black curve shows the signals obtained from the central area of the micro-channel plate (MCP), which was locally damaged by the relatively large number of beam irradiations. The MCP was not new because this measurement was for the pilot

study and we were concerned about damaging the new MCP in the case of a beam handling error. In all cases, the horizontal spreads of the $^{40}\text{Ar}^{8+, 9+, 11+}$ beams were estimated as about 70 mm.

From the PPEM measurement, not only the beam profile but also the emittances were measured. In Fig. 7, the three plots from top to bottom in the left column show the x - y , x - x' , and y - y' projections of the transverse phase-space distribution of the $^{40}\text{Ar}^{11+}$ beam. The top figure shows the hollow triangular beam profile with three intense areas. These are likely to originate from the plasma in the ECRIS or an aberration of the beam optics [10], but further discussion is outside the scope of this report. By selecting each intense area shown in the top row of Fig. 7, the corresponding x - x' and y - y' emittances are shown below each of the profiles. It can be seen that each beamlet occupies specific x - x' and y - y' areas by gating in the x -

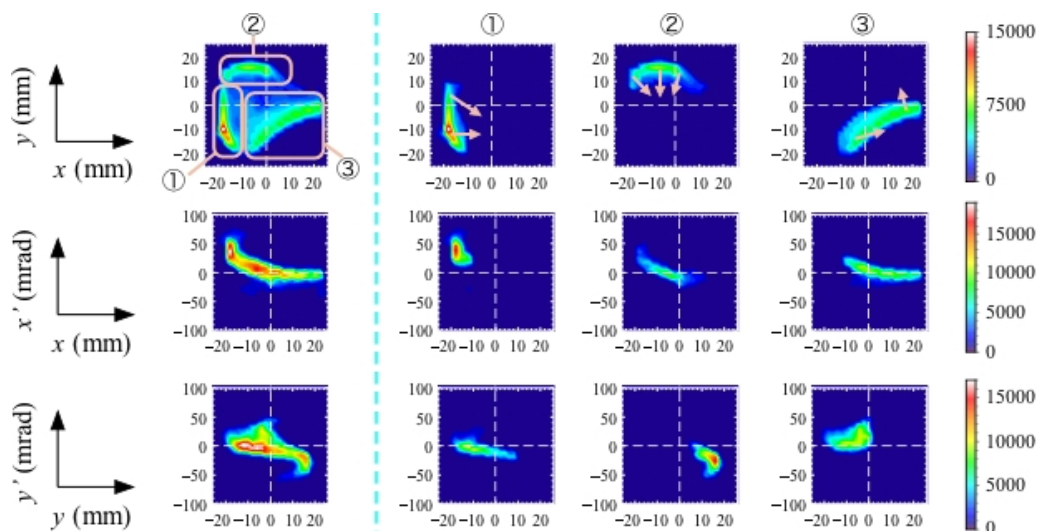


Figure 7: Contour plots showing the projections of the transverse phase-space distribution of the $^{40}\text{Ar}^{11+}$ beam measured by the PPEM. The top, middle, and bottom rows show the x - y , x - x' , and y - y' projections, respectively. In the left column, the x - y projection has a hollow triangular shape with three intense areas. The emittance in each area marked by a red rectangle is illustrated in the three columns on the right. The red arrows show the directions in which the beam components move as the beam progresses along the beam axis.

Content from this work may be used under the terms of the CC BY 3.0 licence (© 2018). Any distribution of this work must maintain attribution to the author(s), title of the work, publisher, and DOI.

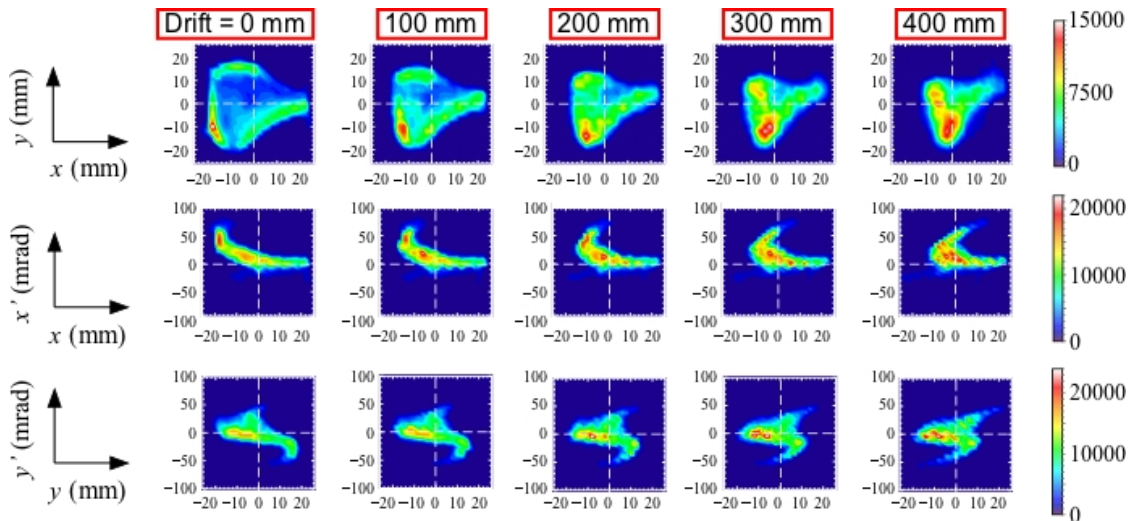


Figure 8: Contour plots showing the simulated evolution of the shape of the $^{40}\text{Ar}^{11+}$ beam (top), the $x-x'$ emittance (middle), and $y-y'$ emittance (bottom) as a function of the drift length from the PPEM. The drift length is provided at the top of each column. The triangular intense beamlets are estimated to converge at a position about 400 mm downstream from the PPEM.

y area only. Taking both the $x-x'$ and $y-y'$ emittances into account, as the beam progresses along the beamline, the beamlets are estimated to move in the directions indicated by the red arrows shown in the top row of Fig. 7. The four-dimensional phase-space distribution was taken into account to simulate the $^{40}\text{Ar}^{11+}$ beam shape evolution with respect to the drift length downstream of the PPEM, as shown in Fig. 8. The movement of the three intense areas of the beam profile is not as simple as those shown in Fig. 7; however, the intense areas are estimated to converge onto an area $30\text{ mm} \times 30\text{ mm}$ square at around 400 mm downstream from the PPEM. As shown in Fig. 8, the transverse phase-space distribution provides essential information for evaluating the validity of the beam optics devices in the immediately downstream LEBT to improve the transport efficiency in the future.

LOW-ENERGY BEAM TRANSPORT

A new LEBT will connect the new ECRIS to the RFQ of the RILAC. The LEBT configuration is as follows: pair solenoid (PSol)–triplet quadrupoles (TQs)–first focal plane (F1)–TQs–second focal plane (F2)–PSol, as

shown in Fig. 9. The PSol consists of two coils with mutually opposing polarities to cancel out the beam rotation induced by the axial magnetic field in the lens. By using a combination of TQs and PSols in the latter half of the LEBT, the horizontal and vertical acceptances at F1 corresponding to those of the RFQ were designed to be an upright ellipse with spatial and momentum axes of 7.4 mm and 19.6 mrad, respectively. The beam transport is optimized to easily fit the acceptance ellipse at F1 using the PSol and TQs in the first half of the LEBT even when the horizontal and vertical focal points are different from each other. The envelopes of the optimized beams with emittances of 145, 200, and 300 $\text{mm} \times \text{mrad}$ are shown at the bottom of Fig. 9. The typical emittance of the beam extracted from the RIKEN 28-GHz ECRIS was measured as $\sim 200\text{ mm} \times \text{mrad}$. From the viewpoint of long-term machine protection from very-high-beam-intensity operation, the beam located outside of the acceptance ellipse needs to be blocked. A set of three horizontal and vertical slits, called triplet slits, will be placed around F1 for this purpose, as shown in Fig. 10. Of course, a spatial slit only provides a vertical limitation in phase space; however,

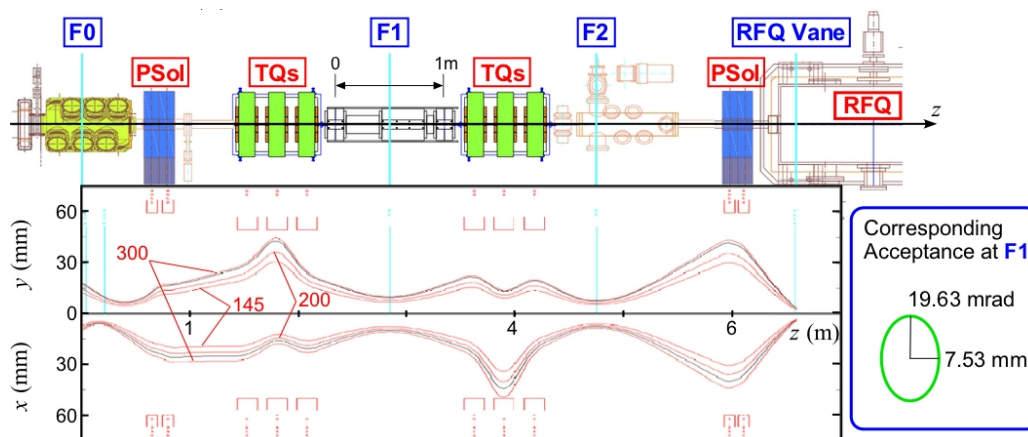


Figure 9: Schematic of the new LEBT (top) and the beam envelopes for which the emittances are assumed as 145, 200, and 300 $\text{mm} \times \text{mrad}$ (bottom). The beam transport is optimized to fit the acceptance at F1, which corresponds to the RFQ acceptance.

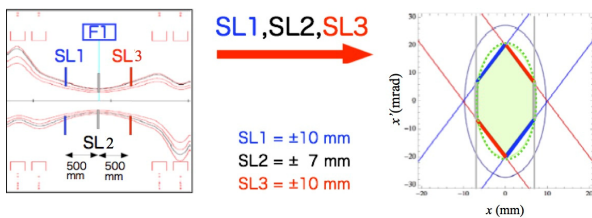


Figure 10: Emittance limitation imposed by triplet slits. The horizontal and vertical slits were located at not only F1 (SL2) but also 500 mm upstream and downstream from F1 (SL1,3). The phase-space limitations by slits SL1, SL2, and SL3 are indicated by blue, grey, and red lines, respectively. By collimation, the beam is confined within the corresponding acceptance at F1 (green dotted ellipse) in Fig. 9.

after a certain drift along the beam axis, the limitation is tilted in proportion to the degrees of x' or y' . Also, by placing a slit at F1, two more slits 500 mm upstream and downstream of F1, with adequate openings, impose a hexagonal limitation, as shown on right side of Fig. 10.

To check the validity of the triplet-slit limitation, we performed 3-D beam tracking with magnetic field mapping by the finite element method. The initial beam was assumed as having a Gaussian distribution in $x-x'$ and $y-y'$ phase space with an emittance of $200 \text{ mm} \times \text{mrad}$. The tilt angles of the emittance ellipses were assumed to be same as those of the envelop calculation in Fig. 9. The results of the tracking simulation with and without the triplet-slit limitation are shown in the top and bottom, respectively, of Fig. 11. From the beam trajectory in Fig. 11, the divergent beam component, which is seen around the RFQ vane region in the no-limitation case, is suppressed by the triplet-slit limitation at F1. Details of the phase space plot show that a small tail still remains, and this is considered to be induced by the aberration of the last PSol because the beam was designed to be widely spread in the lens to fit through the small spatial acceptance of the RFQs, for example, $\pm 3.59 \text{ mm}$.

Fabrication of the beam optics devices, that is, the PSols and TQs, is already complete. The LEBT is now under construction, and we plan to complete it by the end of 2018. After that, we plan to evaluate the validity of the beam optics using an actual beam and PPEM measurements.

SUMMARY AND FUTURE PERSPECTIVES

Construction of the new ECRIS and LEBT for the RILAC was started in 2017 to provide high-intensity beams of ions such as Ca and Zn for nuclear research, and V and Cr for the synthesis of SHEs with $Z > 118$. Because of the very short development period, the new ECRIS has the same structure as the RIKEN 28-GHz SC-ECRIS. With 18-GHz microwave heating, an ^{40}Ar beam was successfully extracted from the new ion source even though several beam optics magnets were incomplete. Using the PPEM, we measured not only the size of ^{40}Ar beams with charge states of 8+, 9+, and 11+, but also the transverse phase space distribution. Especially in the case of the

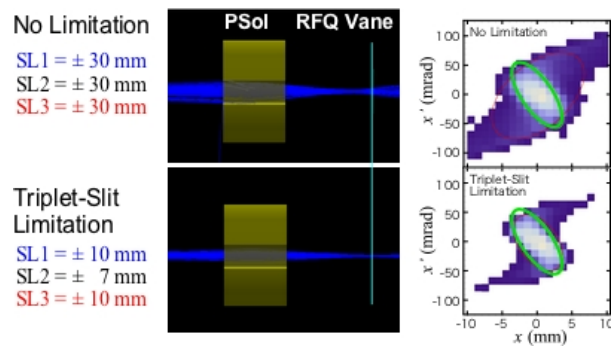


Figure 11: Simulated beam trajectory between the second PSol and the RFQ vane, and the $x-x'$ distribution at the RFQ vane showing the acceptance (green ellipses). Top and bottom panels show the results of simulations with and without the triplet-slit limitation, respectively. The slit limitation at F1 suppresses the divergent component; however, a small tail remains because of the aberration of the PSol.

Ar^{11+} beam, realistic evolution of the beam shape along the beamline was simulated by taking the phase space distribution into account. The LEBT is designed to match the RFQ acceptance and consists of PSol-TQ-TQ-PSol magnets. In addition, the triplet slit located around F1 limits the phase space to block the beam outside the acceptance ellipse. From a 3-D beam tracking analysis, the validity of this limitation was confirmed; however, the beam still has a small tail induced by aberration in the last PSol lens.

Completion of all the remaining components, including the 28-GHz gyrotron, the solenoid at the exit of the ECRIS, and the LEBT, is planned by the end of 2018. After that, we will evaluate the triplet-slit limitation using an actual beam and PPEM measurements. Furthermore, a compact HT oven will be installed, and we will produce metallic beams using highly charged Ca, Ti, and Zn ions, as well as a very intense Cr beam in the future.

REFERENCES

- [1] E. Ikezawa *et al.*, *Proceedings of the 13th International Conference on Heavy Ion Accelerator Technology (HIAT2015)*, Yokohama, Japan, 222 (2015)
- [2] Y. Yano, *Nucl. Instrum. and Meth. B*, vol. 261, p.1009 (2007),
- [3] T. Nakagawa *et al.*, *in these proceedings*.
- [4] T. Nakagawa *et al.*, *Rev. Sci. Instrum.*, vol. 81, p. 02A320 (2010).
- [5] Y. Higurashi *et al.*, *Rev. Sci. Instrum.* vol. 85, p. 02A953 (2014).
- [6] G. D. Alton and D. N. Smithe, *Rev. Sci. Instrum.* vol. 65, p. 775 (1994).
- [7] J. Ohnishi *et al.*, *in these proceedings*.
- [8] M. Leitner *et al.*, *Proceedings of the 15th International work-shop on ECR Ion Source (ECRIS2002)*, Jyväskylä, Finland (2002), unpublished.
- [9] V. Tzoganis *et al.*, *Proceedings of the 13th International Conference on Heavy Ion Accelerator Technology (HIAT2015)*, Yokohama, Japan, vol. 250 (2015),
- [10] Y. Batygin *et al.*, *RIKEN Accelerator Progress Report* vol. 28, p.170 (1995).